

EFFECTS OF GATE EDGES ON VERTICAL VIBRATIONS OF GATES

By

Kiyoshi Takamura
NEWJEC Inc., Osaka, Japan

Hiroyoshi Togashi
Nagasaki University, Nagasaki, Japan

and

Yasushi Hirayama
Nagasaki University, Nagasaki, Japan

SYNOPSIS

The forcibly oscillated model tests of gates have been conducted for seventeen kinds of geometries which had been systematically selected.

Distributions of the amplitude of hydraulic pressure underneath the gate (ΔP_i) have been measured and the phases of the displacement to that of dynamic pressure (β_i) are analysed. The characteristic relations between ΔP_i and β_i are also discussed.

The correlations of the damping coefficients (\bar{C}) versus reduced velocities ($V_r = V/fD$) are given. The experiments show that the negative damping occurs both in the ranges of lower reduced velocities and in relatively high reduced velocities in some cases.

The vibration characteristics for each geometry are compared. Superposition or cancellation by the combination of features involved in three fundamental variations (bevelling, lip installation and rounding of the leading edge) are discussed.

INTRODUCTION

The paper is concerned with the hydraulic forces and the vertical vibrations in underflow gates submerged in free surface flow. Many works have been devoted to the study in this field over the last fifty years and the mechanisms of the vibration phenomenon are finally explained after Naudascher (6), (7) as the following.

(1) In the range of lower reduced velocities :

The excitation is induced by the vortices due to the dynamic interaction between the oscillated gate and the unstable shear layer underneath the gate.

(2) In the range of relatively high reduced velocities :

The excitation is due to the energy input from flow water to the vibration system called " Galloping " of bluff body.

In order to study this vibration phenomenon, two kinds of model systems have been utilized. One is elastic gate model and another is the forcibly oscillated gate model. In the former case, the difficulties can not be avoided in the points of how to apply the similitude law and how to appreciate Coulomb friction between the gate and side walls. In the latter case, Bhargava (1) tested using forcibly oscillated gate models by four kinds of gate geometries. In the tests, the hydraulic pressure underneath the gates was measured, however, the phases of the displacement to that of hydraulic pressure were not treated. Imamura (2) tested using the same system for two kinds of gate geometries and measured the hydraulic pressure and the phases to that of the gate displacement. Negative damping coefficients \bar{C} were also analysed. However, the spaces of transducers were rather wide and the distributions of ΔP_i and β_i underneath the gate were not discussed.

In this report, seventeen kinds of gate geometries are systematically selected and the amplitudes of hydraulic pressure are measured closely. The distributions of ΔP_i and β_i underneath the gate are shown and the relations between both values are investigated.

It is shown that the most effective variation of gate edge to avoid negative damping is bevelling. The vibration characteristics of each geometry are classified into four categories by the combination of signs of \bar{C} values in the lower and the higher ranges of reduced velocities. The study permits several conclusions to be useful in the practical design of gates free from vibrations.

GATE EDGES EMPLOYED

Figures of gate edges normally comprise the following variations such as 1) bevelled on the gate bottom, 2) bottom with a lip, 3) rounding corner at the leading edge and seventeen kinds of edges combined with these variations are employed. These edges are shown in Table 1.

Test results for [F] · [P15] · [M15] which are fundamental types were reported in 1989 (4), and for [LM15] · [LDF] · [LUF] · [LP15] were in 1990 (5) by the authors.

In this paper, test results of other ten kinds of edges are presented. It is considered that all kinds of edges which have been commonly used are included in these variations.

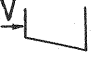
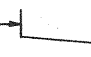


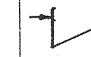
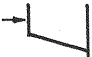

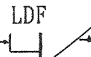
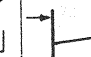



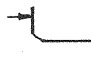

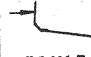
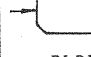
EXPERIMENTS

1.1 Instruments, Apparatus and Test Conditions

A gate body fabricated in plexiglass was installed at the center of the open channel 15 m long, 0.8 m wide and 0.8 m high and was directly oscillated by a mechanical vibration system with an electric motor and a crank as shown in Photo.1. Clearances were covered with rubber seals between the gate and the sides of the channel and the leakage through the gap was found from pressure measurements to have a negligible influence.

The depth of gate is 10 cm and the radius of the corner at the leading edge is fixed to $r = 1.0$ cm referring to a scale of practical gate. The lips are made out of 0.3 cm on thickness aluminium plates. Five sets of pressure sensors and a dynamic strain amplifier of electronic auto-balanced type having six channels are used.

Table 1 Geometries of gate edges investigated

Bevelled angle (α) degree		-30	-15	0	+15	+30
Without rounded	Without lip	 M30	 M15	 F	 P15	 P30
	Lipped (L)	 LM30	 LM15	 LDF LUF	 LP15	 LP30
Rounded corner (R)	Without lip	 RM30	 RM15	 RF	Symb. \rightarrow means flow direction	
	Lipped (L)	 RLM30	 RLM15	 RLDF		

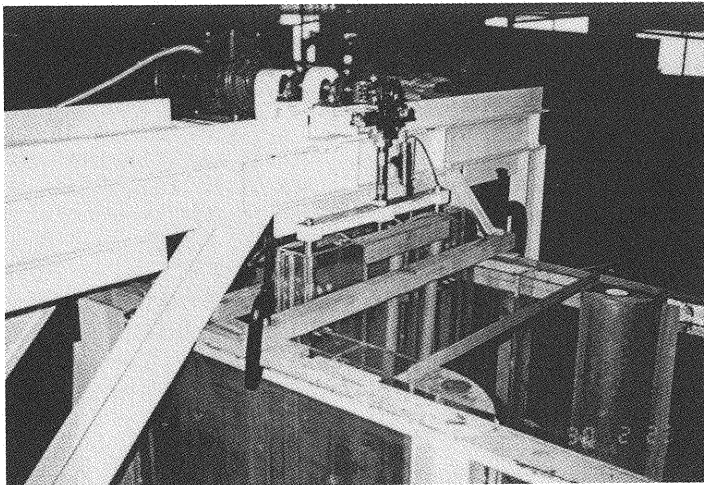


Photo. 1 Test rig and model gate

Arrangements of pressure sensors on gate bottom are shown in Fig.1.

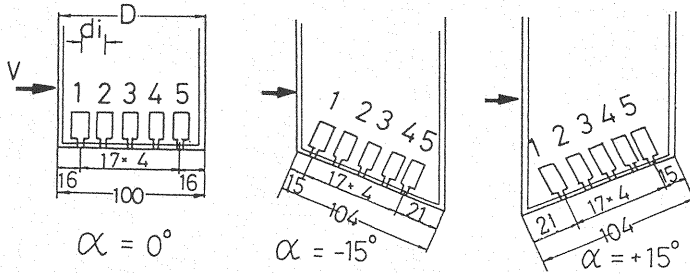


Fig.1 Arrangement of sensors

The scale ratio of modeling is assumed to be nearly 1 : 30. Before the main tests, it was confirmed that approaching flow to the gate was free from turbulences.

Gate opening (s) : Clearances between the gate bottom edge and the bottom surface of the flume were adjusted to be nearly 5.0 cm which were somewhat different depending on the test cases. This small opening was decided referring to the test results by Naudascher (6) in which the flow excited instabilities were experienced always at the conditions of $S/D \approx 0.5$;

Frequency of oscillation (f) : 2~7 Hz ;

Differences of water depth between upstream and downstream sides of gate (ΔH) : 5~40 cm.

Upstream water depth is adjusted from 30 cm to 70 cm by a inflow valve and downstream water depth is adjusted from 20 cm to 30 cm by a flume end shutter to produce a submerged underflow condition in all cases.

Amplitude of oscillation (a) : 5 mm.

In the pre-tests for [F] · [P15] · [M15] (4), amplitudes (a) were adjusted to 0.5, 1.0, 3.0, 5.0 mm and the results of tests showed that values of $\Delta P_i / \gamma \Delta H$ were nearly proportional to the amplitude (a) and related curves of $\bar{C} \sim V_r$ had nearly the same characteristics in each case and were not affected by the amplitude (a). Therefore, the further experiments were limited to 5 mm of amplitude. Here, the notations ΔP_i , γ , \bar{C} , V_r mean the amplitude of local hydraulic pressure, weight of water per unit volume, dimensionless damping coefficient, reduced velocity and the suffix i means the number of sensors.

1.2 Processing of Test Data

Data were recorded and processed by a personal computer. The data sampling time was kept within 25.6 s. and the range of sampling frequency was limited to 80 Hz. Phases of the gate displacement to that of hydraulic pressure were analysed by their cross spectrums.

is deviated from a sinusoidal wave and many small peaks other than the dominant

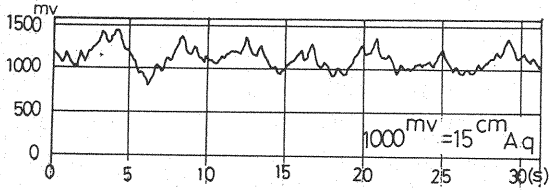


Fig.2 Example of unsteady hydraulic forces

peak of forced oscillation appeared in a power spectrum. Therefore, the pressure amplitude ΔP_i is analysed as the root mean square value of a wave amplitude and made dimensionless after divided by $\gamma \Delta H$.

From Eq.9, \bar{C} becomes positive or negative depending on the distribution of $\Delta P_i / \gamma \Delta H$ and $\sin \beta_i$ along the gate bottom.

2.1 Flat Bottom Type [F]

Distributions of $\Delta P_i / \gamma \Delta H$ and β_i along the gate bottom in each case of reduced velocity V_r are shown in Fig.3 (a).

Distributions of β_i :

In the lower range of V_r ($V_r < 4.0$), β_i distributes like inverse form of character S, and $\sin \beta_i$ is positive around the leading side and is negative around the trailing side. On the other hand, in the higher range of V_r ($V_r > 7.0$), β_i distributes like smoothed airfoil form and β_i is smaller than 180° all over the bottom areas. However, as V_r is increased, β_i becomes negative at the leading edge and in the range of $V_r > 14$, β_i becomes negative all over the areas.

Fig.3(b) shows the distributions at several particular values of V_r intermittently.

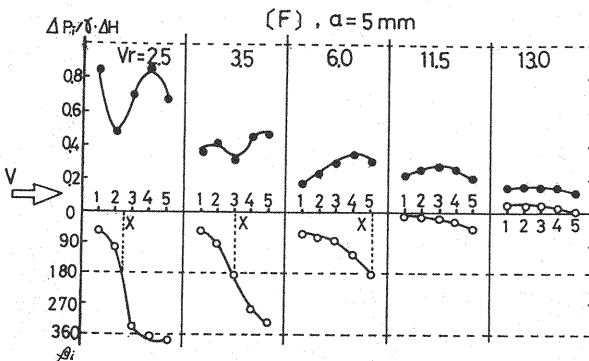


Fig.3(b) Distributions of $\Delta P_i / \gamma \Delta H$ and β_i at several V_r

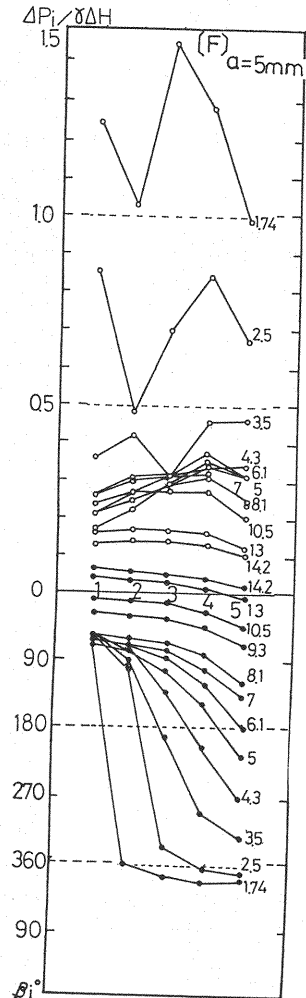


Fig.3(a) Distributions of $\Delta P_i / \gamma \Delta H$ and β_i for different V_r in [F]

If an abscissa where β_i is equal to 180° is designated as point X, the point X shifts from leading to trailing side as V_r is increased and β_i becomes less than 180° all over the areas after all. Here an indicator V_{vcr} is designated as a critical value of the lower range of V_r when the point X reaches just the trailing edge, V_{vcr} is 7.0 in this case. When V_r is larger than V_{vcr} , \bar{C} is always positive.

Distributions of $\Delta Pi/\gamma \Delta H$:

In the lower range of V_r , $\Delta Pi/\gamma \Delta H$ plays the minimum value at the point X and this value becomes smaller as V_r is increased. In the higher range of V_r , this minimum value is disappeared and $\Delta Pi/\gamma \Delta H$ distributes smoothly decreasing to downstream side.

Here $\Delta Pi/\gamma \Delta H$ can be called up by a transport phenomenon intuitively from Fig.3(b). From Eq. 3, if time (t) increases to $(t+\Delta t)$ and phase of $F(t)$ remains still constant, then

$$\omega t - \beta = \omega (t + \Delta t) - (\beta + \Delta \beta); \text{ therefore } \omega \Delta t = \Delta \beta$$

Denote an abscissa along the gate bottom as S and transport velocity as v, then

$$\omega = \frac{\Delta \beta}{\Delta t} = \frac{\Delta \beta}{\Delta S} \cdot \frac{\Delta S}{\Delta t}; \quad v = \lim_{\Delta t \rightarrow 0} \frac{\Delta S}{\Delta t} \quad (10)$$

$$\frac{d\beta}{dS} = \lim_{\Delta t \rightarrow 0} \frac{\Delta \beta}{\Delta S} = \frac{\omega}{v} \quad (11)$$

Gradient $d\beta/dS$ by Eq.11 becomes steep if v is decreased and this suggests that the curve of $\beta_i \sim S$ has a relation with transport velocity. From Fig.3(b), the transport velocity v decreases extremely at the point X.

The curve of $\bar{C} \sim V_r$ is shown in Fig.3 (c). \bar{C} becomes negative in both ranges of the lower velocity of $V_r \approx 4$ and the higher velocity of $V_r > 12$.

Here an indicator V_{gcr} is designated as a critical value of the higher range of V_r where \bar{C} becomes to zero, then $V_{gcr} = 12.0$ in this case. If \bar{C} is anywhere positive, then V_{gcr} does not exist.

However, it was already pointed out that the distribution forms of $\beta_i \sim S$ curves in the lower and the higher ranges of V_r are quite different from each other. This means that the mechanisms of $\bar{C} < 0$ in both ranges of V_r are also different.

Negative damping in the lower V_r is considered to be induced by vortices according to the facts :

- (1) Transport velocity is decreased and ΔPi takes the minimum value at the point X suggesting the reattachment of the vortices to the gate bottom.
- (2) Negative damping occurs within the limited values of V_r suggesting the lock-in phenomenon.
- (3) Strouhal number ($1/V_r$) is nearly 0.2~0.3.

Negative damping in the higher V_r is considered to be induced by the input of flow water energy to vibration system called "Galloping" according to the facts :

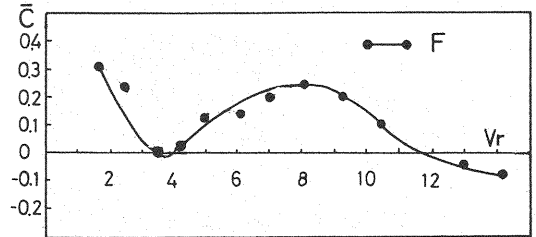


Fig.3(c) \bar{C} versus V_r for [F]

- (1) Strohal number is smaller than 0.1 (relatively lower frequency).
- (2) The distributions of β_i underneath the gate are nearly uniform.
- (3) Negative damping occurs continuously if $V_r > V_{gcr}$.

2.2 Downstream Bevelled Type [P] (Fig.4)

The distributions of $\Delta P_i / \gamma \Delta H$ and β_i along the gate bottom are similar to those of the flat bottom type [F] and the point X is shifted continuously from the leading to the trailing edge as V_r is increased. Comparisons of V_{vcr} and V_{gcr} in these cases are as follows.

	[F]	[P15]	[P30]
V_{vcr}	7.0	5.0	4.0
V_{gcr}	12.0	8.0	7.5

From the above table, if the gate bottom is bevelled to downstream side, the critical values of V_{vcr} and V_{gcr} become smaller than those of [F] and this means that bevelling to downstream side is equivalent to making V_r higher virtually.

When the bevel angle is increased from 15° to 30° , V_{vcr} and V_{gcr} become smaller and $\Delta P_i / \gamma \Delta H$ is decreased.

From the $\bar{C} \sim V_r$ diagram for the case of [P], negative damping in the lower V_r is diminished, however negative damping in the higher V_r still remains.

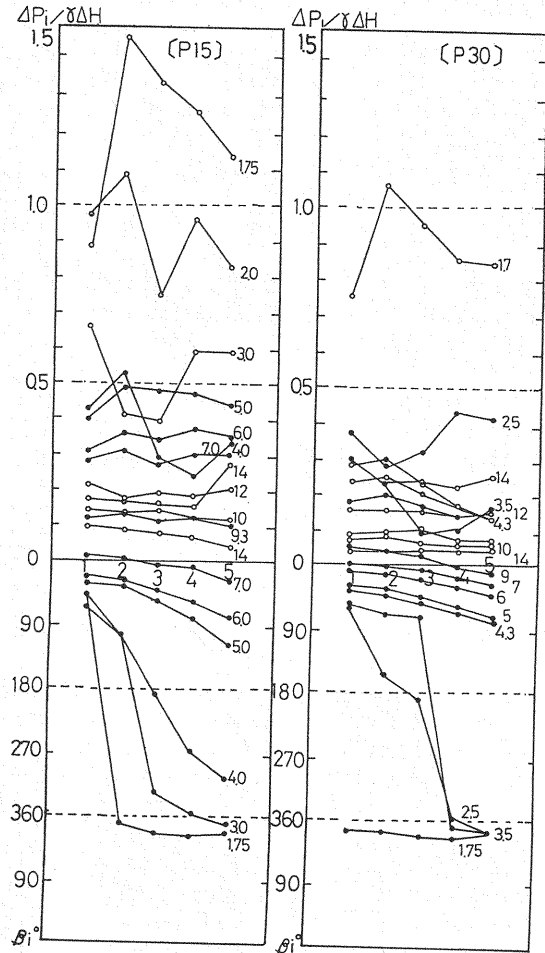


Fig.4(a)(b) Distributions of $\Delta P_i / \gamma \Delta H$ and β_i for different V_r in [P15] & [P30]

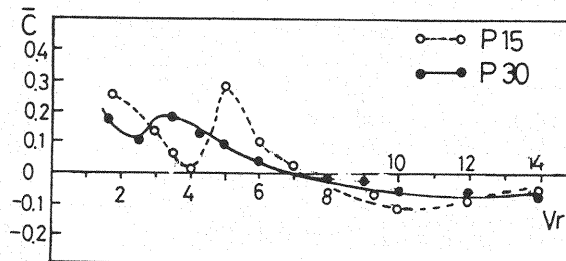


Fig.4(c) \bar{C} versus V_r for [P15] & [P30]

2.3 Upstream Bevelled Type [M] (Fig.5)

In the case of [M15] , V_{vcr} is equal to 9.0 and is different from the case of [P] . Therefore, bevelling to upstream side is equivalent to making V_r lower virtually.

In the case of [M30], the point X can not reach the trailing edge even if V_r is increased. In the case of [M15], the points X are stagnated in three groups of $V_r = 1.75 \sim 3.5$, $4.3 \sim 5.0$ and $6.0 \sim 8.0$. This means that the phenomenon is stationary in a particular range of V_r and is jumped intermittently to the next range of V_r . \bar{C} is positive in both the lower and the higher V_r and this is related by the fact that $\sin \beta_i$ is positive nearly all over the gate bottom excluding narrow negative area.

2.4 Lipped Type [L]

In order to investigate the effects of lip height when the lips are installed at the leading edge [LUF] and at the trailing edge [LDF], a series of tests for models with an extended lip 0.5, 1.0, and 2.0 cm high each was conducted. The results of these tests are shown in Fig.6.

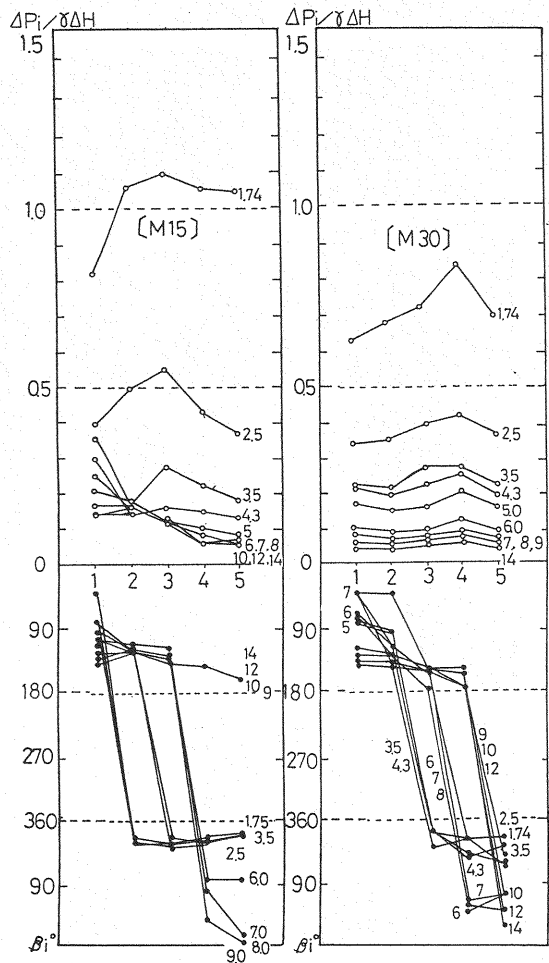


Fig.5(a)(b) Distributions of $\Delta P_i/\gamma \Delta H$ and β_i for different V_r in [M15] & [M30]

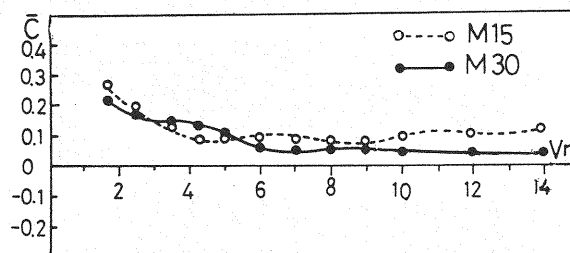


Fig.5(c) \bar{C} versus V_r for [M15] & [M30]

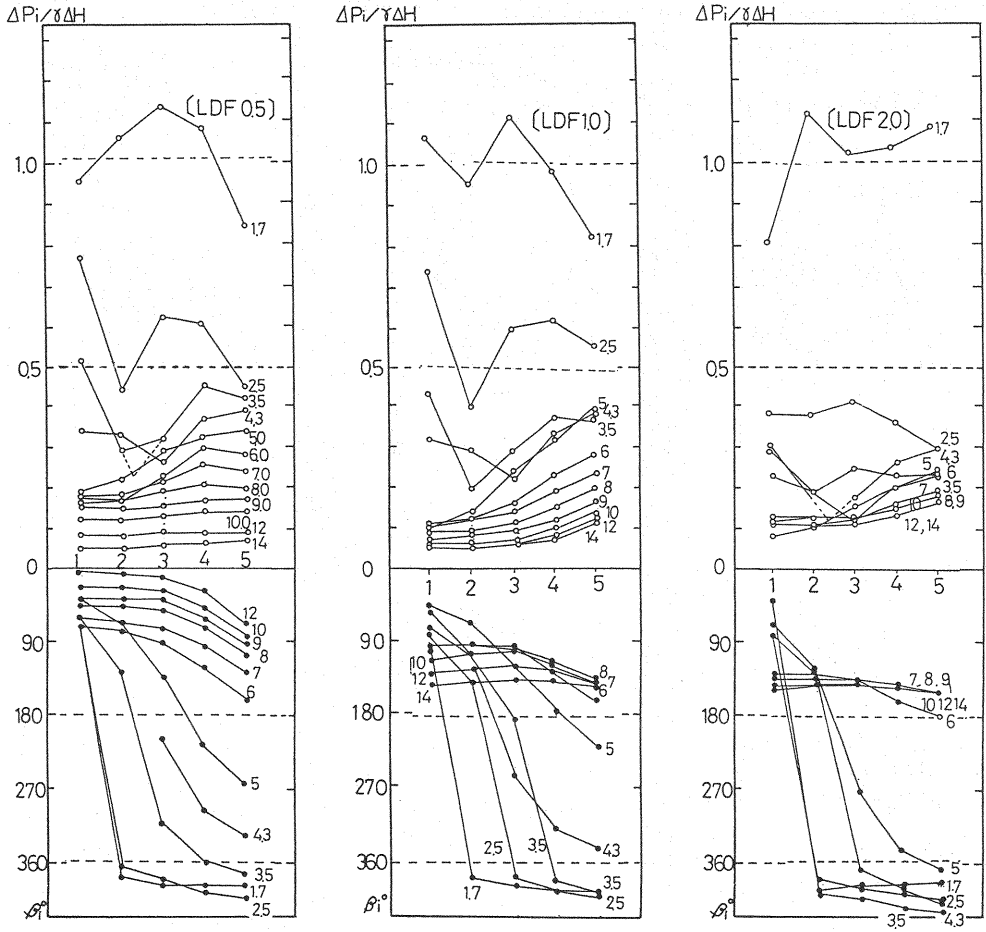


Fig.6(e)(f)(g) Distributions of $\Delta P_i / \gamma \Delta H$ and β_i for lip heights 0.5, 1.0 and 2.0 cm in [LDF]

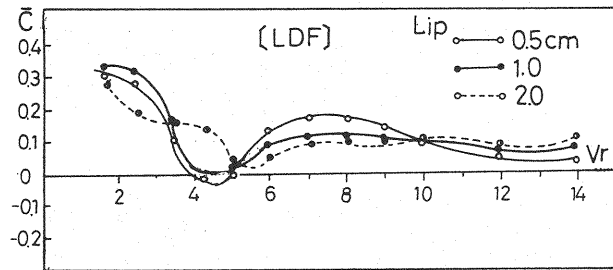


Fig.6(h) \bar{C} versus V_r for lip heights 0.5, 1.0 and 2.0 cm in [LDF]

Comparisons of V_{vcr} and V_{gcr} in each lip height are as follows.

1) Lipped at the leading edge type [LUF]

lip height (cm) :

	0	0.5	1.0	2.0
V_{vcr}	7.0(-)	6.0(-)	5.0(+)	4.3(+)
V_{gcr}	12.0(-)	11.0(-)	9.0(-)	9.0(-)

2) Lipped at the trailing edge type [LDF]

lip height (cm) :

	0	0.5	1.0	2.0
V_{vcr}	7.0(-)	6.0(-)	6.2(+)	6.2(+)
V_{gcr}	12.0(-)	* (+)	* (+)	* (+)

Legend * means that V_{gcr} does not exist. Signs of \bar{C} are shown in ().

From the above comparisons of the values of V_{vcr} , V_{gcr} and the signs of \bar{C} , the followings are observed. For [LUF] and [LDF], the signs of \bar{C} in the lower V_r become positive in the case of lip height 1.0 cm. For [LDF], the signs of \bar{C} in the higher V_r become positive in the case of lip height 0.5 cm. V_{gcr} for [LUF] and V_{vcr} for [LDF] for lip height 1.0 cm are nearly the same values as for 2.0 cm. The effect of lip installation appears at the lip height 1.0 cm and the differences between the cases of lip height 1.0 cm and 2.0 cm are not remarkable. Therefore, further tests for [LP], [LM], [RLDF] and [RLM] are conducted with lip height 1.0 cm only.

3) Lipped type combined with downstream side bevel [LP] (Fig.7)

Comparisons of V_{vcr} and V_{gcr} in each type are shown below.

	[LUF]	[LP15]	[LP30]
V_{vcr}	5.0	3.5	3.0
V_{gcr}	9.0	6.5	6.0

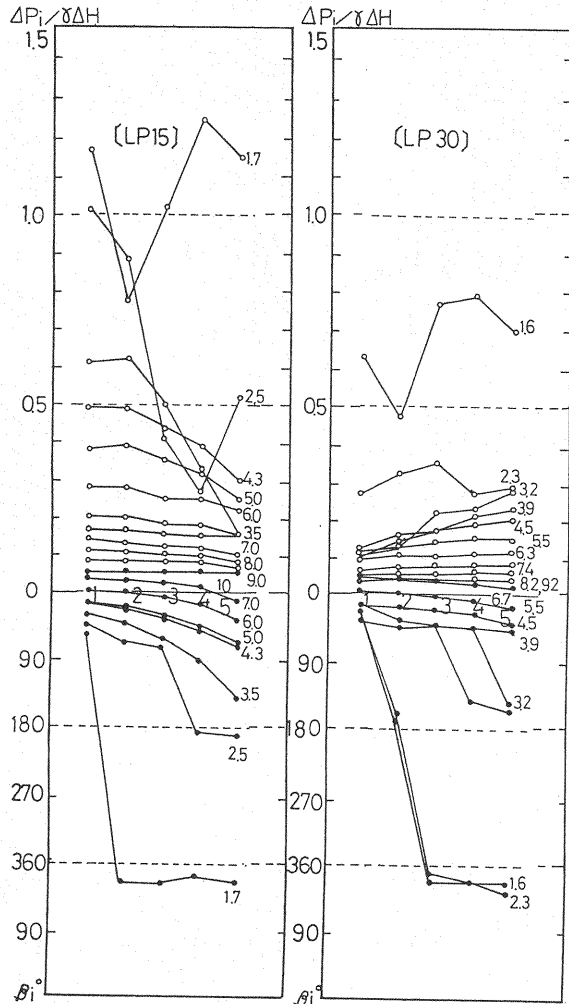


Fig.7(a)(b) Distributions of $\Delta P_i / \gamma \Delta H$ and β_i for different V_r in [LP15] & [LP30]

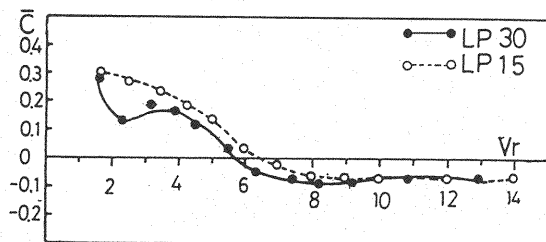


Fig.7(c) \bar{C} versus V_r for [LP15] & [LP30]

Values of V_{vcr} and V_{gcr} in the cases of [LP15] and [LP30] are much smaller than those values in [LUF], [P15] and [P30]. Downstream side bevel and lip installation at the leading edge are both effective to decrease the values of V_{vcr} and V_{gcr} . So, it can be understood that the effects of [L] and [P] are superposed after their combination. By increasing of bevel angle (α) from 15° to 30° , the values of V_{vcr} and V_{gcr} are not so affected.

4) Lipped type combined with upstream side bevel [LM] (Fig.8)

As aforementioned in 2), V_{vcr} and V_{gcr} of [LDF] become positive if the lip is extended more than 1.0 cm as the same as in the case of [M]. Experimental curves of $\bar{C} \sim V_r$ show mildly concaved. The values of \bar{C} for [M] and [LM] at the particular V_r in the lower and the higher ranges are compared as the following.

	\bar{C} in lower $V_r(=2)$	\bar{C} in higher $V_r(=14)$
[M15]	0.25	0.13
[M30]	0.20	0.04
[LM15]	0.35	0.13
[LM30]	0.18	0.06

From the above comparisons, the effects of superposing [L] and [M] can not be found clearly, though the curves of $\bar{C} \sim V_r$ in [M] and [LM] are similar. By increasing of bevel angle (α) from 15° to 30° , the values of \bar{C} are reduced to nearly a half.

2.5 Rounded Corner Upstream Side

It can be expected that rounded corner upstream side is similar to [M] hydraulically. Due to hydraulic conditions, such three cases shall be expected that stream lines do not separate or separate at the corner and also, though separate, a point of separation is from time to time fluctuating.

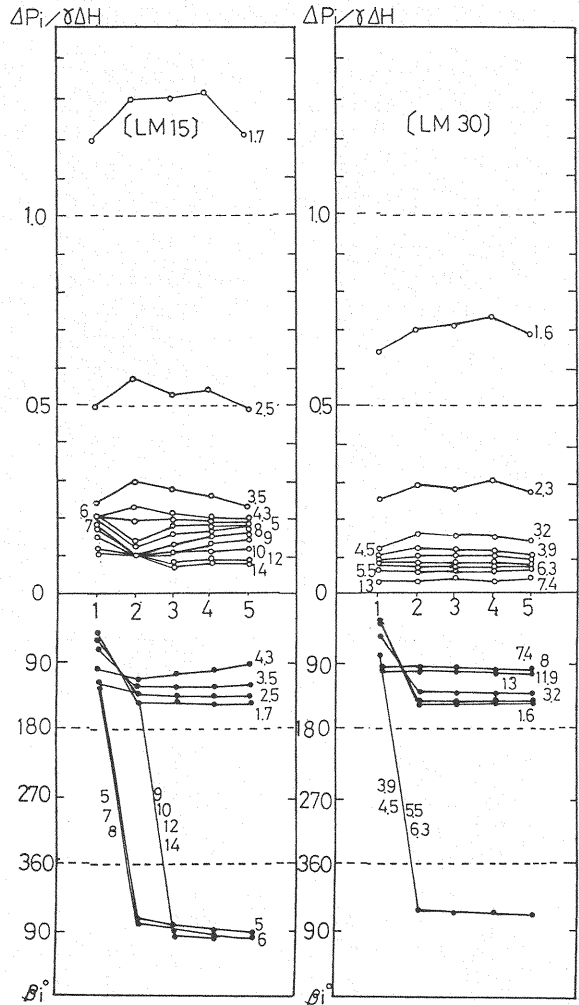


Fig.8(a)(b) Distributions of $\Delta P_i / \gamma \Delta H$ and β_i for different V_r in [LM15] & [LM30]

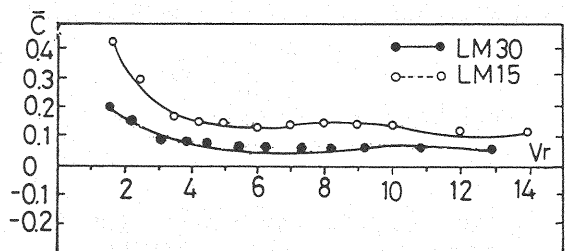


Fig.8(c) \bar{C} versus V_r for [LM15] & [LM30]

1) Simple rounded corner type [RF] (Fig.9)

Comparing Fig.9(a) with Fig.3(a), distributions of $\Delta P_i / \gamma \Delta H$ are like those of [F], however the values of $\Delta P_i / \gamma \Delta H$ are reduced to almost 2/3 of [F].

Distributions of β_i are like those of [F], however areas where $\sin \beta_i < 0$ are wider than those of [F] in the higher range of V_r . Accordingly, the curves of $\bar{C} \sim V_r$ are similar to those of [F] and the values of \bar{C} are negative in the lower and the higher ranges of V_r . Consequently, $|\bar{C}|$ are nearly zero and much smaller than those of [F]. The characteristics of [RF] are somewhat like [F], however [RF] exhibits the effect to diminish those characteristics of [F].

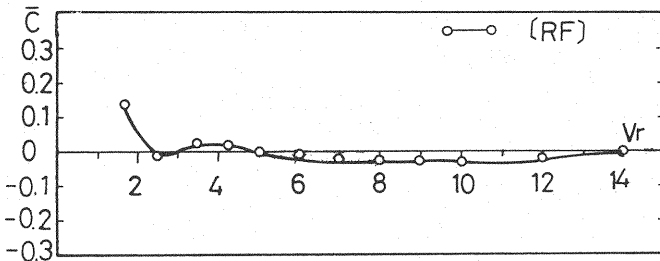


Fig.9(b) \bar{C} versus V_r for [RF]

2) Rounded corner combined with upstream side bevel [RM] (Fig.10)

In the cases of [RM15] and [RM30], the distributions of $\Delta P_i / \gamma \Delta H$ and β_i in the lower range of V_r are nearly the same as of [M]. However, the distributions of β_i in the higher range of V_r show particular forms of $\beta_i > 180^\circ$ for [RM15] and, on the other hand, [M] type for [RM30].

Consequently, $\bar{C} \sim V_r$ curves for [RM15] are like those of [P] in the points that \bar{C} values are positive in the lower V_r and negative in the higher V_r and absolute value of \bar{C} in the higher V_r are nearly zero. [RM30] is similar to [M]. In this case, the feature of $\bar{C} \sim V_r$ curve in [RF] is diminished.

3) Rounded corner combined with lip [RLDF] (Fig.11)

Distributions of $\Delta P_i / \gamma \Delta H$ and β_i are similar to those of [M] and consequently the characteristics of $\bar{C} \sim V_r$ curves in [RF] of Fig.9 (b) or [LDF] of Fig.6(h) are lost after the combining of [RF] with [LDF].

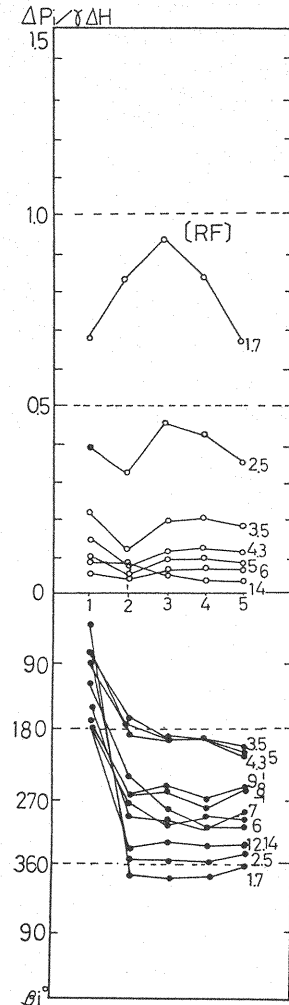


Fig.9(a) Distributions of $\Delta P_i / \gamma \Delta H$ and β_i for different V_r in [RF]

- 4) Rounded corner combined with lip and downstream side bevel [RLM] (Fig.12)

$\Delta P_i / \gamma \Delta H$ is decreased at the leading edge commonly in [R]. The characteristics of [RLM15] are similar to those of [M15] and the characteristics of [RLM30] are equal to those of [RM30] or [M].

Superposition of the characteristics involved in [RF], [LDF] and [M] after their combining is not effective.

2.6 Classification of Vibration Characteristics of Gate Edges

The vibration characteristics of various kinds of gate edges are classified into four types of [M], [P], [LDF] and [F], according to the combination of signs of \bar{C} in the lower and the higher ranges of V_r .

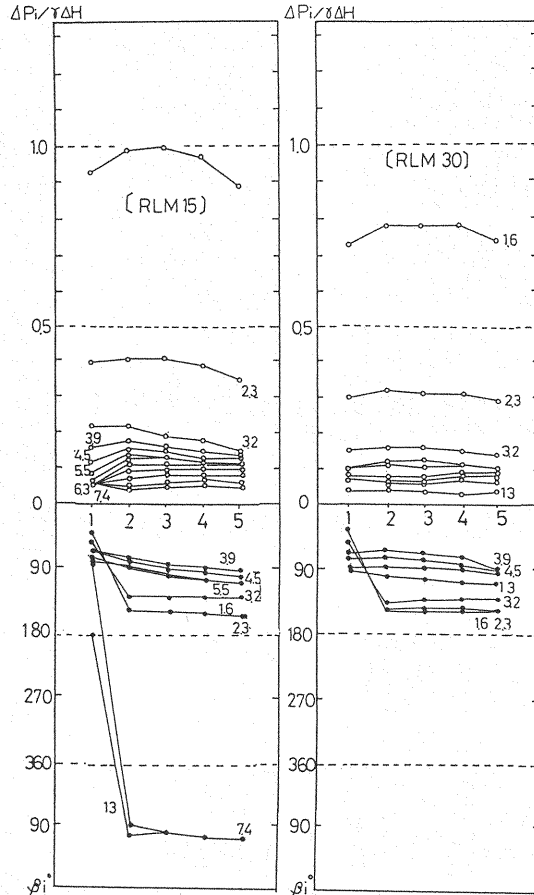


Fig.12(a)(b) Distributions of $\Delta P_i / \gamma \Delta H$ and β_i for different V_r in [RLM15] & [RLM30]

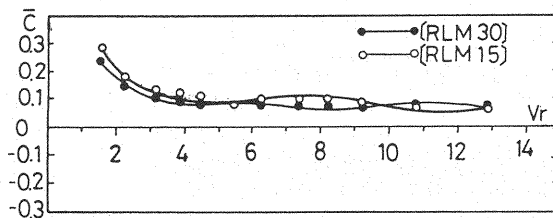


Fig.12(c) \bar{C} versus V_r for [RLM15] & [RLM30]

	sign of \bar{C} in the lower V_r	sign of \bar{C} in the higher V_r
[M]	+	+
[P]	+	-
[LDF]	-	+
[F]	-	-

By this classification, the characteristics of seventeen kinds of gate edges which have been tested are summarized in Table 2.

Table 2 Summary of vibration characteristics of seventeen kinds of edges tested

Type	Gate edges
[M]	M15, LM15, RM30, RLDF, RLM15 M30, LM30, RLM30
[P]	P15, LUF, LP15, RM15 P30, LP30
[LDF]	LDF
[F]	F, RF

CONCLUSIONS

The vibration characteristics of gate edges can be appreciated from the distribution forms of $\Delta P_i / \gamma \Delta H$ and β_i along the surface of gate bottom and by the resultant curves of $\bar{C} \sim V_r$.

These characteristics behave differently in the lower and the higher ranges of V_r and the critical values for the lower and the higher ranges of V_r are designated by V_{vcr} and V_{gcr} .

Synthetic conclusions of the experiments for seventeen kinds of gate edges are as follows.

1) Vibration characteristics of each edge type are classified into four categories of the type [M], [P], [LDF] and [F] by the combination of signs of \bar{C} in the lower and the higher ranges of V_r .

2) The most effective type to avoid negative damping in three fundamental variations (bevelling, lip installation and rounding of the leading edge) is bevelling of gate bottom and when bevelled angle (α) is increased from 15° to 30° , the followings are observed :

from	to	
[P15]	→ [P30]	Bevelling becomes more effective ;
[M15]	→ [M30]	the same as the above ;

APPENDIX-NOTATION

The following symbols are used in this paper :

- a = forcibly oscillated amplitude ;
- c' = hydraulic damping coefficient ;
- \bar{C} = integrated damping coefficient ;
- d_i = spacing of pressure sensors ;
- D = depth of gate ;
- f = forcibly oscillated frequency ;
- F = unsteady hydraulic force ;
- ΔH = water level difference between upstream and downstream water depth ;
- i = pressure measurement point number ;
- k' = hydraulic spring constant ;
- m' = virtual mass ;
- ΔP_i = R.M.S value of hydraulic pressure amplitude ;
- s = gate opening ;
- S = abscissa along the gate bottom ;
- t = time ;
- v = transport velocity ;
- V = flow velocity at the gate opening ;
- V_r = reduced velocity ;
- V_{vcr} = indicator meaning a critical velocity in the lower V_r ;
- V_{gcr} = indicator meaning a critical velocity in the higher V_r ;
- X = gate displacement ;
- α = degree of inclination in gate bottom ;
- β = phase of gate displacement to that of hydraulic force ;
- β_i = phase of gate displacement to that of local hydraulic pressure ;
- γ = weight of water per unit volume ; and
- ω = angular frequency of oscillation.

(Received November 9, 1992; revised January 29, 1993)